Paraffin-Based Reconfigurable Antenna Operating at 100 GHz

Behnam Ghassemiparvin®, *Member, IEEE*, and Nima Ghalichechian®, *Senior Member, IEEE*

Abstract—A paraffin-based frequency reconfigurable antenna operating at 100 GHz is reported in this article. Paraffin is a mechanical phase-change material (PCM) that undergoes reversible solid-liquid volumetric change of approximately 15%. In addition, due to its low dielectric loss, this material is suitable for certain electromagnetic applications such as antennas at the millimeter-wave band often defined as 30 to 300 GHz. In this work, paraffin-based micro actuators forming variable capacitors are integrated with a slot antenna structure. Here, paraffin is encapsulated with a dielectric layer and actuated using a Joule heater. A variable capacitor is formed between a metal layer patterned on top of the paraffin and the ground layer. Following multi-physics simulation steps, prototype antennas are fabricated and tested. With a low actuation voltage of 5.4 V, 1.4 μm of displacement and 15.3% change in capacitance are achieved. Actuation and switch off time of the device is found to be 5.7 ms and 1.8 ms, respectively. Performance of the reconfigurable antenna is evaluated through on-wafer probe measurements. The antenna covers the bandwidth of 94.1–104.1 GHz ($S_{11} < -10$ dB) and the resonance frequency shift of 6.8 GHz is achieved. Applications of such reconfigurable antenna includes wireless communication, radars, and biomedical imaging.   [2020-0180]

Index Terms—MEMS, millimeter wave (mmW), multiphysics, paraffin, phase-change material, reconfigurable antenna, slot antenna.

I. Introduction

MILLIMETER-WAVE (mmW) communications (30–300 GHz) offer a very high bandwidth to accommodate for the demands of media-rich mobile devices. Reconfigurability and adaptability are crucial features of the future millimeter-wave communication systems. Reconfigurable antennas are essential elements that facilitate the smart utilization of spectrum and space through frequency, pattern, and polarization reconfiguration. However, implementation of reconfigurable antennas at the mmW band provides significant challenges in the design, fabrication, and testing steps.

Behnam Ghassemiparvin was with the ElectroScience Laboratory, Department of Electrical and Computer Engineering, The Ohio State University, Columbus, OH 43212 USA. He is now with Apple Inc., Cupertino, CA 95014 USA (e-mail: ghassemiparvin.1@osu.edu).

Nima Ghalichechian is with the ElectroScience Laboratory, Department of Electrical and Computer Engineering, The Ohio State University, Columbus, OH 43212 USA (e-mail: ghalichechian.1@osu.edu).

Color versions of one or more of the figures in this article are available online at http://ieeexplore.ieee.org.

Digital Object Identifier 10.1109/JMEMS.2020.3013159

As the wavelength is in the order of a few millimeters, antenna size shrinks significantly. As a result, integration of discrete reconfiguring elements such as diodes becomes extremely challenging. Therefore a monolithic integration is required to avoid electromagnetic losses. Moreover, biasing lines for tunable elements need to be miniaturized to minimize the RF interference. Another challenge is the intrinsic ohmic and dielectric losses of the elements that increase at higher frequencies. Tuning elements such as PIN diodes [1], [2], Gallium-Arsenide (GaAs) switches [3], and varactors [4], have series resistance $> 4\Omega$ which has a significant effect on the radiation efficiency of these antennas. Materials with variable permittivity such as liquid crystals and barium strontium titanate (BST), suffer from dielectric losses due to their loss tangent values higher than 0.01. In addition, they require high voltage in order to achieve the full reconfiguration range [5]. RF MEMS switches and variable capacitors have a very low resistance which makes them highly efficient and they can be fabricated monolithically with the antennas [6]. Though, they require high actuation voltages, yet their operation is limited to two discrete states; therefore, they are incapable of continuous tuning as needed in most applications. Ohmic switches based on phase-change materials (PCM) such as germanium-telluride [7] and vanadium dioxide [8], [9] exhibit low insertion loss, but similar to MEMS switches, they mostly operate at two states.

At microwave frequencies ($f < 30$ GHz), PIN [10] and varactor [4], [11] diodes are used to achieve reconfiguration by changing the electrical length or the physical length of the antenna. Although, semiconductor switches and capacitors have a very fast response time and lower bias voltage, due to their lower series resistance, RF MEMS switches are more efficient. At lower frequencies, these switches can be integrated as discrete packaged elements [12], however, monolithic integration reduces the losses [6], [13]. In addition, conventional printed circuit board (PCB) techniques can be combined with microfabrication to achieve a hybrid monolithic integration [14], [15]. By introducing more reconfiguring elements, multifunctional antennas with pattern, frequency and polarization reconfiguration can be achieved where the antenna aperture is reshaped by switching electrically small patch elements [16], [17]. On the other hand, increasing the tuning elements increases the losses, which is critical in mmW antennas.

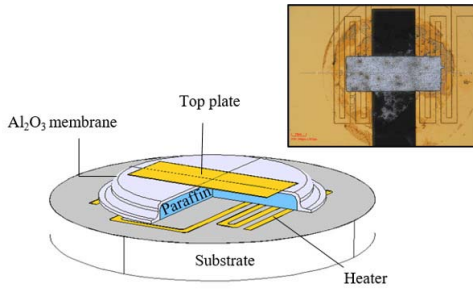Achieving reconfiguration at mmW band is extremely challenging due to the micron-level feature size, integration

Fig. 1. Detailed view of the paraffin PCM variable capacitor. Micrograph of the fabricated capacitor is shown in the inset.

Fig. 2. Micrograph of the fabricated bent slot antenna with two paraffin PCM-based tunable capacitors.

and increased conductive and dielectric losses. Conventional MEMS switches are used to achieve discrete frequency reconfiguration by changing the electrical length of a slot antenna [6]. For instance, due to the discrete operation of the MEMS switch, antenna is limited to four states covering the frequency range of 28-35 GHz. In [18], Schottky varactor diode is integrated with an annular slot antenna using flip-chip bonding to achieve a continuously reconfigurable antenna at 200 GHz. However, flip-chip bonding is not a monolithic process. Due to the bulky size of the diode chip compared to the antenna, only one diode can be used. As a result, reconfiguration range of the antenna is limited to 3 GHz. In order to reduce the dielectric losses, a pneumatically actuated patch antenna with air filled cavity substrate is proposed in [19]. However, integrating a pneumatic system is extremely difficult and not reliable. In addition, even though a very large mechanical displacement of 187% is achieved, a limited frequency change of 4 GHz (51–55.3 GHz) is achieved. Optical switches can be used to modify the slot length in a slotted waveguide array to achieve frequency reconfiguration [20]. Even though, optical switches do not require any biasing line, they are activated by external laser source that makes the integration challenging. In addition, optical switches only have two discrete states and cannot provide a continuous tuning.

To address the aforementioned challenges, we introduce a new class of reconfigurable RF microsystems using paraffin PCM. This novel microsystem offers low-loss, continuous reconfiguration that can be monolithically integrated with mmW antennas and RF components. Paraffin or alkane is a mechanical PCM that exhibits a reversible (approximately 15%) volumetric change during its solid-liquid transition [21]. Large volumetric change of paraffin creates a large force and displacement that can be used in micro-actuators [22]–[24]. However, in our work, in addition to the mechanical displacement, we take advantage of the low dielectric loss of paraffin to form a variable capacitor. As previously reported by our group, due to its non-polar chemical structure, paraffin has a loss tangent of $\tan \delta = 6.6 \times 10^{-4}$ at 110 GHz [25], [26]. As shown in Fig. 1, a micro-heater embedded below a paraffin-held cavity generates the heat required to control the volumetric change. The gradual change in distance between the membrane and ground, which is dependent on the heater generated temperature, forms a continuously-variable capacitor between the metallic membrane and the ground plane.
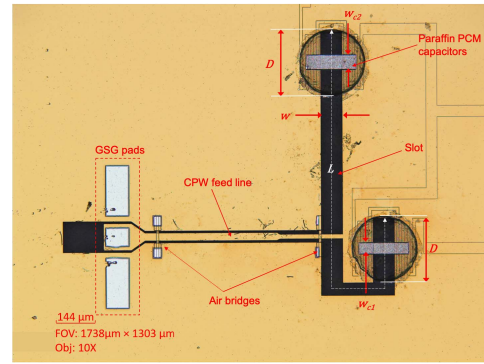
We have monolithically integrated these variable capacitors with a slot antenna to achieve frequency reconfiguration. Fig. 2 shows the micrograph of the fabricated reconfigurable slot antenna. By loading the antenna with the paraffin PCM capacitors, the electrical length of the slot changes resulting in a varying resonance frequency. A key challenge in such tunable systems is that reconfiguration leads to excessive losses [27]. Here, we base our concept on a bent slot design at microwave frequencies [28] and our earlier simulation study on the paraffin antenna [29], [30].

In this work, we show the design, simulation, fabrication and testing of the paraffin-based reconfigurable mmW antenna operating at 100 GHz. The paper is organized as follows: In Section II a brief description of the antenna design is given. Section III is focused on the thermo-electro-mechanical actuation and multiphysics simulation, followed by the details of a six-layer microfabrication process for the device. RF and mechanical displacement measurements of the device are given in Section V, and summary of the paper is provided in Section VI.

II. ANTENNA DESIGN

Structure of the antenna is shown in Fig. 2 where a bent slot antenna is loaded with two paraffin PCM variable capacitors to achieve frequency reconfiguration. The slot has a length of one wavelength or λ which it is operated at its second resonance frequency. Bent shape is adopted to avoid radiation pattern null at broadside. Loading the slot line with two capacitors changes the propagation constant along the line. Therefore, the electrical length of the antenna changes which results in a shift in the resonance frequency. The location of the variable capacitors along the slot is optimized using a circuit model adopted from [11] to achieve the maximum frequency shift for 15% capacitance change.

A summary of antenna dimensions are given in Table I. To operate at 100 GHz, total length of the antenna is 1.52 mm with a width of 80 μm. Capacitors are positioned at 113 μm (approximately $\lambda/12$) from the shorted edges. Paraffin PCM capacitors are actuated using integrated heaters. These heaters are positioned under the ground plane to minimize the coupling to the RF and degradation of the antenna performance. Antenna is fed with a off-centered coplanar waveguide (CPW)

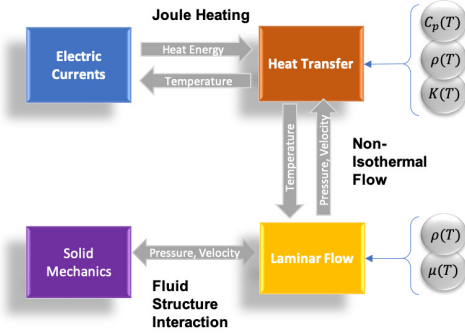| w	L	D	w_{c1}	w_{c2}	Paraffin thickness
80	1520	120	58	70	2.6

Fig. 3.   Flow chart of the fully coupled multiphysics simulation for paraffin PCM actuator.
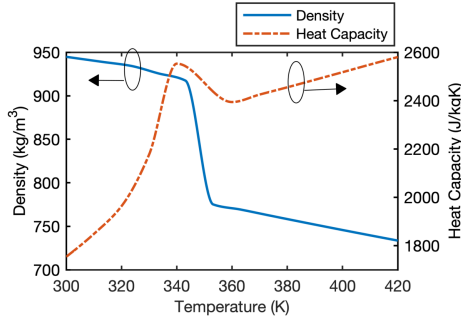
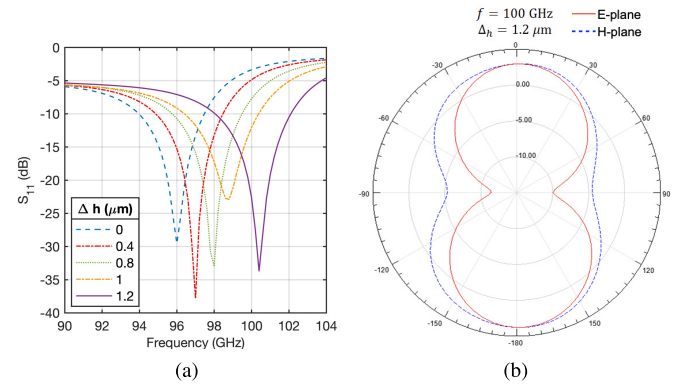Fig. 4.   Temperature dependent density and heat capacity of hexatriacontane.

Fig. 5.   (a) Simulated reflection coefficient of the reconfigurable slot antenna for various displacement values of the paraffin PCM capacitor. (b) Simulated radiation pattern of the antenna for displacement of 1.2 μm at 100 GHz.

transmission line. In order to suppress the parasitic coupled slot line mode ground equalizing bridges are used at the antenna feed location and the discontinuities along the CPW transmission line [31].

III. MULTIPHYSICS SIMULATION FOR THE PARAFFIN PCM CAPACITOR

To evaluate the actuation performance of paraffin PCM device, multiphysics simulation is carried out in COMSOL by coupling the electrical energy, heat convection, conduction, laminar flow, and mechanical motion. A flow chart of the multiphysics simulation is shown in Fig 3. Paraffin is modeled as a liquid with temperature dependent density, viscosity, heat capacity, and heat conductivity. Density, heat capacity, viscosity and thermal conductivity of the hexatriacontane, which is a type of paraffin are considered as temperature dependent. Heat capacity and density with respect to the temperature are shown in Fig. 4 [32]. Phase transition temperature of the hexatriacontane is 348 K (75°C) where its density decreases significantly. In addition, maximum value for the heat capacity at this temperature, is due to the latent heat of the phase transition.

In the multiphysics model, first, current is calculated using the AC/DC module according to the applied voltage. Next, generated heat energy is coupled to the Heat Transfer module through Joule heating. In addition, temperature is coupled back

to the AC/DC module to account for the change in the conductivity of the heater. Temperature distribution is calculated in all of the regions except paraffin, using thermodynamic heat transfer in solids. Fluid thermodynamics is required for paraffin, since it is modeled as liquid. To couple the heat from solids to the liquid paraffin, surface to surface radiation is considered and surface emissivity is defined for all of the surfaces encapsulating the paraffin. For the surfaces that are exposed to the ambient air, a constant convective heat flux density of 5 W/m^{2}K is defined which is a typical value for a low speed flow of air over a surface. Substrate, except its top surface, is assumed to be at a constant temperature of 20°C.

To calculate the pressure inside the paraffin cavity, Laminar Flow module is used and non-isothermal flow is considered. Paraffin's viscosity and density are temperature dependent as the temperature is coupled from the Heat Transfer module through non-isothermal flow. Once the pressure is calculated, it is coupled to the Solid Mechanics module using fluid-structure interaction. Solid mechanics module calculates the exerted force on the encapsulating layer and the top metal plate and consequently, displacement is calculated. This displacement is used in full-wave electromagnetics simulation using ANSYS HFSS to model the variable capacitors. Fig. 5(a) shows the simulated reflection coefficient of the antenna for various center displacements. Antenna covers the frequency band of 94 GHz–102.2 GHz (S_{11} < -10 dB) and the resonance frequency shifts by 4.6 GHz. Antenna has a dynamic impedance bandwidth of 4.1 GHz (S_{11} < -10 dB). Radiation pattern of the antenna for the center displacement of 1.2 μm is illustrated in Fig. 5(b). Since the current distribution does not change significantly, radiation pattern of the antenna remains approximately constant for various displacement values and has a maximum gain of 3 dBi at 100 GHz. Considering simulated displacement profile for capacitors and no roughness for paraffin layer, total efficiency of the antenna is 66% and 71% for max displacement of 0 μm and 1.4 μm, respectively.

3D schematic of the actuator is shown in Fig. 1. The heat source is a Joule heater which consists of a 250 nm-thick and 10 μm-wide meandered gold line and excited with a DC voltage of 2 V. Gold is used due to the availability and the reliable microfabrication processes. In addition, using other
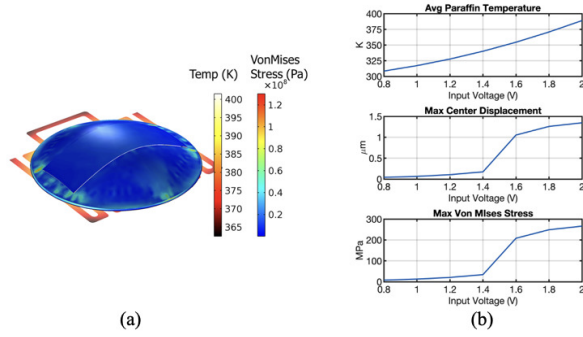
Fig. 6. (a) Simulated Von Mises stress and temperature distribution of the paraffin PCM actuator with input voltage of 2 V. (b) Simulated Average paraffin temperature, maximum center displacement, and maximum Von Misses stress of the paraffin PCM capacitor for input voltage of 0.8–2 V.
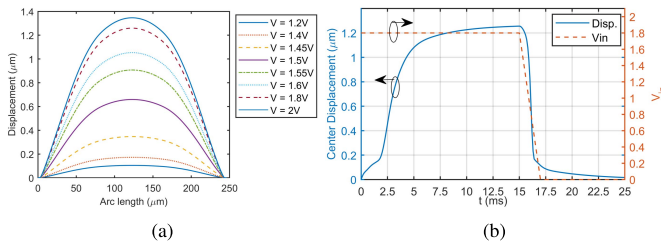

Fig. 7. (a) Simulated deflection profile of the paraffin PCM actuator for input voltages in the range of 1.2–2 V. (b) Simulated transient response of the peak displacement for input voltage of 1.8 V showing actuation time of 5.7 ms and switch-off time of 1.8 ms.
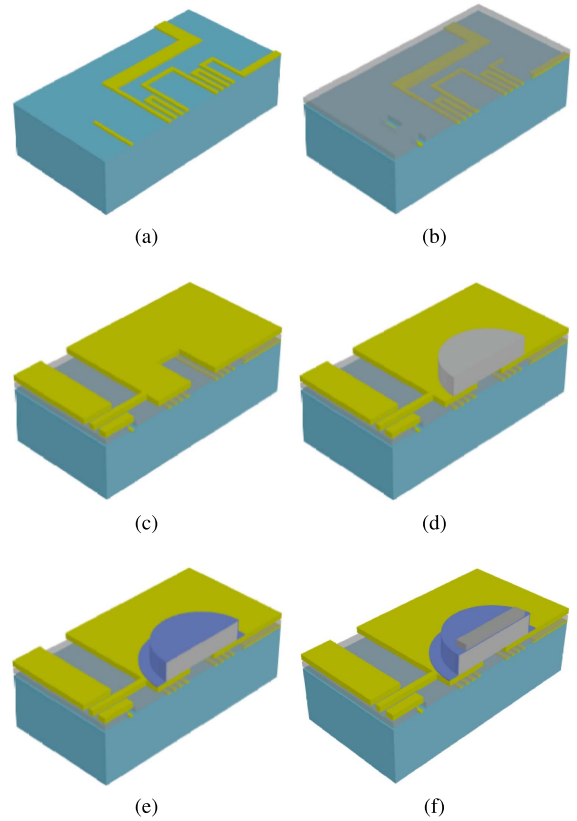

Fig. 8. 3D illustration of the microfabrication process for (a) layer 1: heater, (b) layer 2: insulator, (c) layer 3: ground plane, (d) layer 4: paraffin, (e) layer 5: encapsulation, and (f) layer 6: capacitor.

material with lower conductivity would not provide a significant advantage over gold and would increase the complexity of the fabrication process. The temperature distribution of the heat source is shown in Fig. 6. Average paraffin temperature for input voltage of 2 V reaches 115°C (389 K) which is well above the phase transition temperature of hexatriacontane (75°C). Von Mises stress for the encapsulating layer of aluminum oxide (Al_2O_3) is also depicted in Fig. 6(a) that has a maximum value of 120 MPa which is well below the yield stress of the material.

Stationary simulation results of the paraffin PCM device are shown in Fig. 6. Phase transition of paraffin occurs at the input voltage of approximately 1.4 V where the temperature reaches 348 K (75°C). A rapid increase in the displacement and the paraffin pressure can be observed after the phase transition.

Fig. 7(a) shows the deflection profile of the actuator for various heater input voltage. Actuator reaches its peak displacement of 1.35 μm for input voltage of 2 V. According to the transient response of the PCM device given in Fig. 7(b), actuation time is found to be 5.7 ms and switch off time is 1.8 ms.

IV. FABRICATION

The device is fabricated using a six-layer photolithography process on a 200 μm-thick quartz substrate. Overview of the fabrication process is shown in Fig. 8. First, integrated heaters are fabricated by patterning a 250-nm thick layer of gold using lift-off process followed by 1 μm of SiO_2 for electrical isolation. SiO_2 is deposited using plasma-enhanced chemical

vapor deposition and dry etched using CF_4. Both the antenna and the feeding lines are fabricated using 750 nm-thick layer of gold (lift-off process). Thickness of the gold is determined as three times the skin depth at 100 GHz.

An in-house spin coating process used for the deposition of a 2.6 μm-thick layer of paraffin [33]. Solution for the paraffin deposition is prepared by dissolving solid paraffin pallets in p-xylene and heating to 65°C. In addition, in order to maintain the solution in the liquid phase, spin coating is performed using a substrate heated to 120°C. During spin coating solution cools down and forms the paraffin film. After deposition of the paraffin, process temperatures are maintained below 65°C to avoid reflowing. To etch paraffin, a photoresist etch mask is deposited using a low temperature photolithography process. The paraffin is etched using O_2 plasma with inductively coupled reactive ion etcher. Substrate is cooled down to 10°C during this process.

To contain the paraffin in liquid phase during actuation, a conformal coating is required. Paraffin is encapsulated with a 75 nm-thick layer of Al_2O_3 that is deposited using atomic layer deposition (ALD). Trimethylaluminium (TMA) and water are used as precursors. Standard deposition temperature for Al_2O_3 is at 300°C in our tool, however, to deposit on paraffin layer, substrate temperature is decreased to 65°C. In addition, to promote the growth at 65°C, ALD precursor pulse width are increased to 0.5 s.

To obtain a conformal layer, sputter deposition is used for the top metal layer. The top plate for the capacitor is fabricated
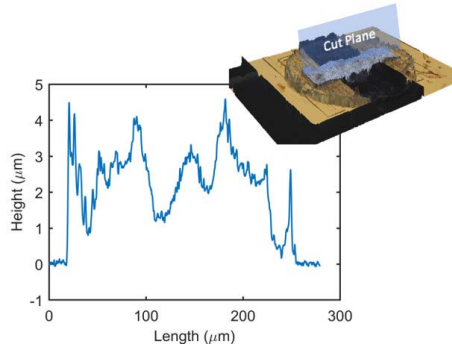
Fig. 9. Measured thickness profile of the fabricated paraffin PCM actuator.

by a 750 nm-thick layer of aluminum and patterned using wet etching.

The major challenge is the surface roughness of the paraffin layer. A profile measurement of the actuator is carried out using NanoScience Zeta-20 3D optical profilometer and it is shown in Fig. 9. Paraffin layer has a average thickness of 2.4 μm, however, thickness varies in the range of 1.3–4 μm. Paraffin layer has a very uneven surface, consequently, deposited aluminum layer is also has high roughness. To decrease the roughness, after encapsulation, paraffin film is reflowed and gradually cooled down, nevertheless, it does not have a significant effect on the roughness. In order to decrease the roughness, a carrier wafer can be used to increase the heat capacity of the substrate, so that the substrate can retain the heat during spin coating and resulting paraffin film would have smoother surface. Our team carried out a detailed study of the paraffin deposition and the surface roughness in [33] for various substrates and spin parameters.

V. EXPERIMENTAL RESULTS

To characterize the paraffin PCM actuator and the reconfigurable slot antenna, mechanical displacement of the microactuator, resistance of the integrated heaters and the input impedance of the reconfigurable antenna are measured.

A. Displacement Measurement of the Paraffin PCM Microactuator

Displacement of the paraffin microactuator is measured using an optical profilometer. Picture of the measurement setup is shown in Fig. 10. Initially, to actuate the device, an external polymide insulated heater (Omega Engineering, Inc.) was used. External heater is excited with a DC voltage of 52 V (current of 60 mA). The maximum temperature of 80°C is achieved. Temperature is monitored using a type K thermocouple probe which is placed 20 mm away from the device to avoid any damage. Profile measurements are carried out with a 50× lens with a maximum height resolution of 0.012 μm. Note that optical profilometer used here is capable of accurately measure a reflective material. Consequently, only profile of the top metal layer can be measured.

3D profile of the device is shown in Fig. 11 for actuated and unactuated states. One dimensional profiles of the device along the capacitor's top plate is shown in Fig. 12(a). Comparison between the measured displacement (height difference
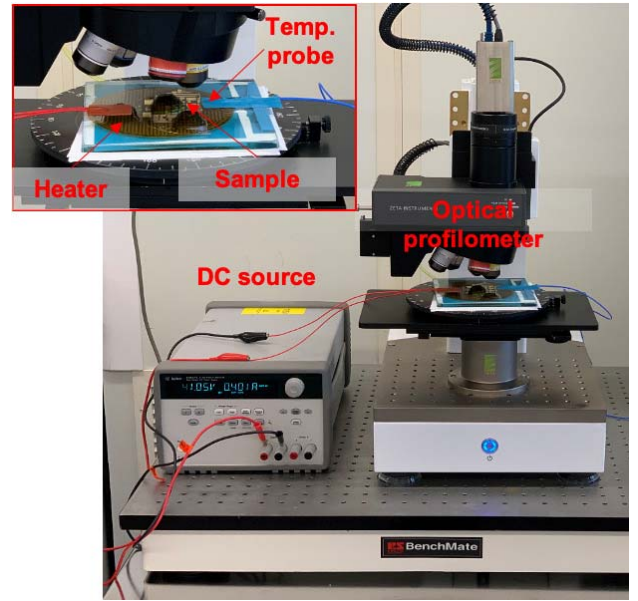

Fig. 10. Setup for profile measurement of the paraffin PCM actuator. Detailed view of the sample, heater, and the temperature probe is shown in the inset.
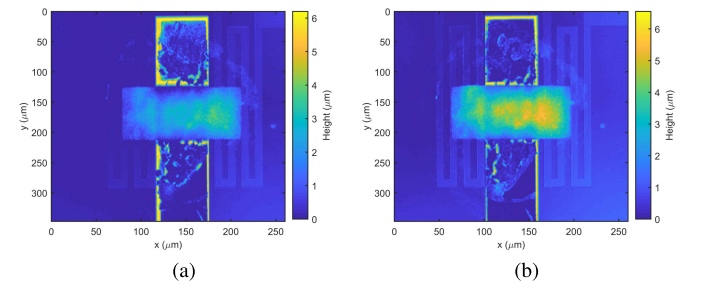

Fig. 11. Measured 3D profile of the paraffin PCM capacitor at (a) 20°C (not actuated) and (b) 80°C (actuated).

between two states) and the simulated displacement for input heater voltage of 2 V (which has the maximum displacement) is shown in Fig. 12(b). It can be seen that there is a close agreement between the measured and the simulated value and maximum displacement of 1.4 μm is achieved. Accuracy of the measurement is affected by the rough surface of paraffin. In addition, heat generated by the profilometer's microscope changes the temperature of the actuator and results in variation of the profile as it scans the height. While systematic reliability studies are outside the scope of this article, we have observed that our devices exhibit repeatable actuation performance in laboratory environment.

B. RF Measurements of the Reconfigurable Slot Antenna

To measure the input impedance of the reconfigurable antenna, on wafer measurements are performed using a ground-signal-ground (GSG) waveguide probe (Waveguide Infinity Probe, Form Factor Inc.). Probe has a WR8.0 waveguide input which is connected to a frequency extender (Virginia Diodes Inc., N5262AW08) in conjunction with a Keysight network analyzer (PNA-X N5242A). Measurements are carried out in the frequency range of 90–140 GHz. Experiments are carried out using a Cascade M150 probe station. Measurement setup is shown in Fig. 13.
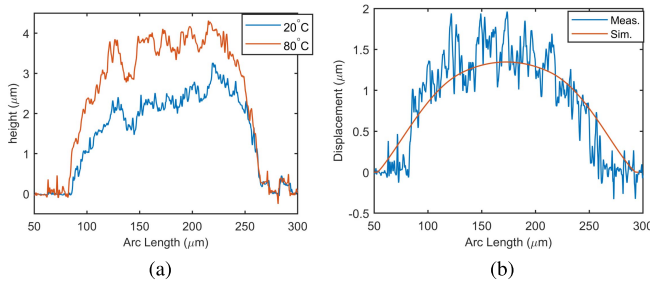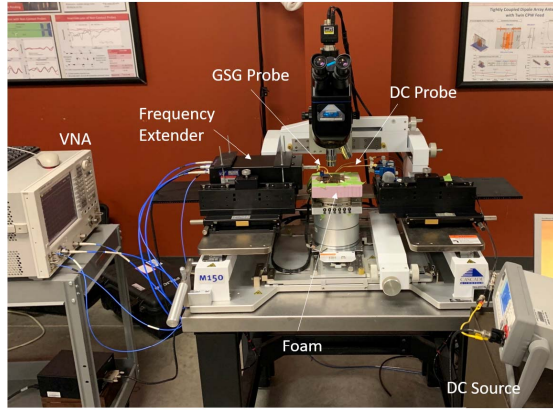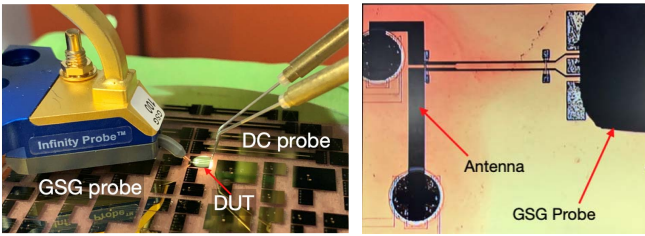
Fig. 12. (a) Measured profile of the paraffin PCM device at 20°C and 80°C. (b) Comparison of the measured displacement with the simulated displacement for input heater voltage of 2 V.

Fig. 13. (a) mmW measurement setup for input impedance measurement of the reconfigurable antenna. (b) Detailed view of the GSG and DC probe positioning. (c) Close-up of the GSG probe and the device under test (DUT).

For the probe-tip measurements, a two-tier calibration is performed. Initially, the network analyzer is calibrated to a reference plane coincided with the waveguide port of the frequency extender. Next, probe-tip calibration is performed by terminating the GSG probe with four CPW offset shorts [34].

Both PCM capacitors are actuated simultaneously using DC probes. DC voltage is applied to the integrated heaters which are connected in series.

Radiation pattern measurement is not performed since such a test at 100 GHz requires overcoming extreme instrumentation challenges such as rotating bulky frequency-extenders and feeding waveguides in three-dimensional space. Even though our group have developed a robotic measurement system at 60 GHz band [35]. Integrating the frequency extenders and maintaining a stable phase reference and stable probe station with the rotating arm at 100 GHz is extremely challenging.

Reflection coefficient of the antenna with input voltage of zero is shown in Fig. 14(a) and antenna has a resonance
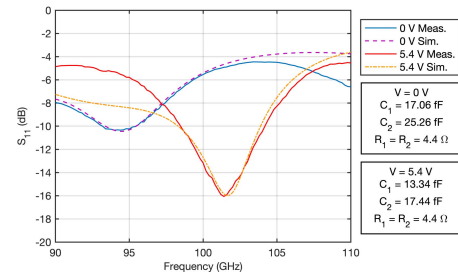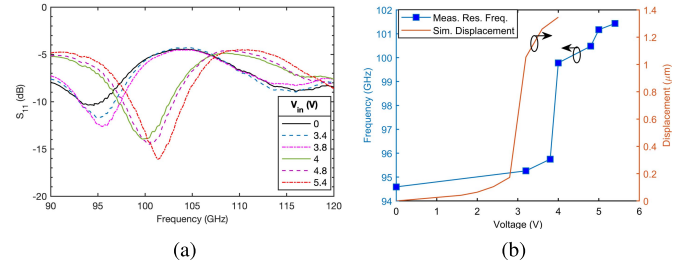

Fig. 14. Measured and simulated reflection coefficient of the reconfigurable antenna for input heater voltage of 0 V and 5.4 V.

Fig. 15. (a) Measured reflection coefficient of the reconfigurable antenna for the input voltage in the range of 0–5.4 V. (b) Measured resonance frequency (frequency of maximum return loss) of the antenna and the simulated displacement of the paraffin PCM capacitor with respect to the input voltage of the heater.

frequency of 94.6 GHz. Capacitance values are extracted using a series lumped model of the capacitor and the full-wave simulation of the slot antenna. For the input voltage of 0 V, capacitance values are found to be $C_1 = 17.8$ fF and $C_2 = 25.3$ fF and estimated resistance value is 4.4 Ω. With the increased resistance, using finite element simulations, total efficiency of the antenna is estimated as 51% and 63% for input voltage of 0 V and 5.4 V, respectively. Reflection coefficient of the antenna at the actuated state is shown in Fig. 14(b). A 5.4 V is applied to the heaters and capacitance values are estimated as $C_1 = 13.4$ fF and $C_2 = 17.4$ fF. Based on this extracted values capacitance ratio of 1.33 is achieved.

Measured reflection coefficient of antenna for input voltage range of 0–5.4 V is depicted in Fig. 15(a). Resonance frequency shifts from 94.3 GHz to 101.6 GHz with the increasing heater voltage.

Frequency shift of the antenna with respect to the input voltage is illustrated in Fig. 15(b). Total frequency shift of 6.8 GHz is achieved. The abrupt change in the resonance frequency in the voltage range of 3.8–4 V is due to the phase transition of the paraffin layer which significant volume change occurs.

Based on the multiphysics simulations shown in Section III, phase transition occurs at heater voltage of 1.4–1.6 V for one of the actuators. Considering that both heaters are identical and have the same resistance, phase transition should occur at 2.8–3.2 V when two heaters are excited in series. However, according to measured data in Fig. 15(b), the phase transition happens at input voltage of 3.8–4 V which is 0.8 V higher than the simulated value. Discrepancy is due to the difference in the simulated model and the device under test. In the simulation, only a finite and small portion of the device is simulated. Thus,

TABLE II

COMPARISON OF MMW RECONFIGURABLE ANTENNAS IN LITERATURE

Reference	Reconfiguring element	No. of elements	No. of states	Variable change (%)	Frequency range	Frequency shift
[18]	Schottky varactor	1	Continuous	Capacitance, 100% (2.4–4.79 fF)	202.7–197 GHz	5.7 GHz
[19]	Pneumatic actuator	1	Continuous	Displacement, 187%, (200–573 μm)	51–55.3 GHz	4.3 GHz
[6]	RF-MEMS	2	4	N/A	28, 29.2, 31.5, 35 GHz	7 GHz
[20]	Photoconductive switch	4	2	N/A	30, 34 GHz	4 GHz
This work	Paraffin PCM Capacitor	2	Continuous	Capacitance, 15%	94.3–101.6 GHz	7.3 GHz

the heat loss to the larger ground plane and air is underestimated. In addition, differences in the ambient temperature and the air flow in the measurement environment contribute to the error. A performance comparison of the paraffin PCM based antenna and the literature is given in Table II. It can be seen that even though paraffin PCM capacitors have a significantly small capacitance change, a very wide reconfiguration range of 7.3 GHz is achieved compared to the literature.

VI. CONCLUSION

In this work, for the fist time we demonstrated, a new class of electrothermally actuated devices based on paraffin phase-change materials. Electrical and mechanical properties of paraffin makes it an attractive material for designing low loss reconfigurable structures at mmW band. Moreover, micromachining facilitates monolithic integration of paraffin PCM capacitors with antennas and RF components. Unlike the classical RF-MEMS devices, paraffin PCM variable capacitors are capable of continuous tuning while maintaining a low-loss performance with a series resistance of less than 0.7 Ω at 100 GHz.

Using these new capacitors, we have realized a reconfigurable antenna operating at 100 GHz capable of frequency tuning in the range of of 94–104.1 GHz. Input impedance of the antenna measured using on-wafer probing and a frequency shift of 6.8 GHz is achieved with a maximum input voltage of 5.4 V. Series resistance of capacitors are extracted to be 4.4 Ω. A good agreement is observed between the simulated and measured return loss.

Displacement of the device was measured using optical profilometer and a maximum displacement of 1.4 μm is achieved. Measured displacement profile shows close agreement with the multiphysics simulation. According to the displacement values, capacitance ratio is calculated as 1.33. Through transient multiphysics simulation, the actuation time for the device was found to be 5.7 ms. Potential applications for such reconfigurable antenna includes radars, communication and imaging.

REFERENCES

[1] S. Genovesi, A. D. Candia, and A. Monorchio, "Compact and low profile frequency agile antenna for multistandard wireless communication systems," *IEEE Trans. Antennas Propag.*, vol. 62, no. 3, pp. 1019–1026, Mar. 2014.

[2] Y. P. Selvam, L. Elumalai, M. G. N. Alsath, M. Kanagasabai, S. Subbaraj, and S. Kingsly, "Novel frequency- and pattern-reconfigurable rhombic patch antenna with switchable polarization," *IEEE Antennas Wireless Propag. Lett.*, vol. 16, pp. 1639–1642, 2017.

[3] T. Aboufoul, A. Alomainy, and C. Parini, "Reconfiguring UWB monopole antenna for cognitive radio applications using GaAs FET switches," *IEEE Antennas Wireless Propag. Lett.*, vol. 11, pp. 392–394, 2012.

[4] C. R. White and G. M. Rebeiz, "Single- and dual-polarized tunable slot-ring antennas," *IEEE Trans. Antennas Propag.*, vol. 57, no. 1, pp. 19–26, Jan. 2009.

[5] R. Reese *et al.*, "A millimeter-wave beam-steering lens antenna with reconfigurable aperture using liquid crystal," *IEEE Trans. Antennas Propag.*, vol. 67, no. 8, pp. 5313–5324, Aug. 2019.

[6] K. Van Caekenberghe and K. Sarabandi, "A 2-bit ka-band RF MEMS frequency tunable slot antenna," *IEEE Antennas Wireless Propag. Lett.*, vol. 7, pp. 179–182, 2008.

[7] L. Chau *et al.*, "Optically controlled GeTe phase change switch and its applications in reconfigurable antenna arrays," *Proc. SPIE*, vol. 9479, pp. 8–15, May 2015.

[8] V. Sanphuang, N. Ghalichechian, N. K. Nahar, and J. L. Volakis, "Reconfigurable THz filters using phase-change material and integrated heater," *IEEE Trans. THz Sci. Technol.*, vol. 6, no. 4, pp. 583–591, Jul. 2016.

[9] D. E. Anagnostou, D. Torres, T. S. Teeslink, and N. Sepulveda, "Vanadium dioxide for reconfigurable antennas and microwave devices: Enabling RF reconfigurability through smart materials," *IEEE Antennas Propag. Mag.*, vol. 62, no. 3, pp. 58–73, Jun. 2020.

[10] D. Peroulis, K. Sarabandi, and L. P. B. Katehi, "Design of reconfigurable slot antennas," *IEEE Trans. Antennas Propag.*, vol. 53, no. 2, pp. 645–654, Feb. 2005.

[11] N. Behdad and K. Sarabandi, "Dual-band reconfigurable antenna with a very wide tunability range," *IEEE Trans. Antennas Propag.*, vol. 54, no. 2, pp. 409–416, Feb. 2006.

[12] G. H. Huff and J. T. Bernhard, "Integration of packaged RF MEMS switches with radiation pattern reconfigurable square spiral microstrip antennas," *IEEE Trans. Antennas Propag.*, vol. 54, no. 2, pp. 464–469, Feb. 2006.

[13] E. Erdil, K. Topalli, M. Unlu, O. A. Civi, and T. Akin, "Frequency tunable microstrip patch antenna using RF MEMS technology," *IEEE Trans. Antennas Propag.*, vol. 55, no. 4, pp. 1193–1196, Apr. 2007.

[14] H.-P. Chang, J. Qian, B. A. Cetiner, F. De Flaviis, M. Bachman, and G. P. Li, "RF MEMS switches fabricated on microwave-laminate printed circuit boards," *IEEE Electron Device Lett.*, vol. 24, no. 4, pp. 227–229, Apr. 2003.

[15] J. Pal *et al.*, "Magnetically-actuated micromechanical nickel patches for a monolithically integrated reconfigurable antenna on printed circuit board," *J. Micromech. Microeng.*, vol. 29, no. 11, Nov. 2019, Art. no. 115020.

[16] A. Grau Besoli and F. De Flaviis, "A multifunctional reconfigurable pixeled antenna using MEMS technology on printed circuit board," *IEEE Trans. Antennas Propag.*, vol. 59, no. 12, pp. 4413–4424, Dec. 2011.

[17] L. N. Pringle *et al.*, "A reconfigurable aperture antenna based on switched links between electrically small metallic patches," *IEEE Trans. Antennas Propag.*, vol. 52, no. 6, pp. 1434–1445, Jun. 2004.

[18] Z. Jiang, J. L. Hesler, S. M. Rahman, L. Liu, and P. Fay, "Tunable 200 GHz lens-coupled annular-slot antennas using Schottky varactor diodes for all-electronic reconfigurable terahertz circuits," *Electron. Lett.*, vol. 49, no. 23, pp. 1428–1430, Nov. 2013.

[19] S. Hage-Ali, N. Tiercelin, P. Coquet, R. Sauleau, V. Preobrazhensky, and P. Pernod, "A millimeter-wave inflatable frequency-agile elastomeric antenna," *IEEE Antennas Wireless Propag. Lett.*, vol. 9, pp. 1131–1134, 2010.

[20] I. F. da Costa, A. Cerqueira S., D. H. Spadoti, L. G. da Silva, J. A. J. Ribeiro, and S. E. Barbin, "Optically controlled reconfigurable antenna array for mm-Wave applications," *IEEE Antennas Wireless Propag. Lett.*, vol. 16, pp. 2142–2145, 2017.

[21] S. P. Srivastava, J. Handoo, K. M. Agrawal, and G. C. Joshi, "Phase-transition studies in n-alkanes and petroleum-related waxes—A review," *J. Phys. Chem. Solids*, vol. 54, no. 6, pp. 639–670, Jun. 1993.

[22] E. T. Carlen and C. H. Mastrangelo, "Surface micromachined paraffin-actuated microvalve," *J. Microelectromech. Syst.*, vol. 11, no. 5, pp. 408–420, Oct. 2002.

[23] M. Lehto, R. Boden, U. Simu, K. Hjort, G. Thornell, and J.-Å. Schweitz, "A polymeric paraffin microactuator," *J. Microelectromech. Syst.*, vol. 17, no. 5, pp. 1172–1177, Oct. 2008.

[24] R. Bodén, M. Lehto, U. Simu, G. Thornell, K. Hjort, and J.-Å. Schweitz, "A polymeric paraffin actuated high-pressure micropump," *Sens. Actuators A, Phys.*, vol. 127, no. 1, pp. 88–93, Feb. 2006.

[25] B. Ghassemiparvin and N. Ghalichechian, "Broadband complex permittivity measurement of paraffin films at 26 GHz–1 THz using time domain spectroscopy," in *Proc. IEEE Int. Symp. Antennas Propag. USNC/URSI Nat. Radio Sci. Meeting*, Jul. 2017, pp. 887–888.

[26] B. Ghassemiparvin and N. Ghalichechian, "Complex permittivity measurement of paraffin phase-change material at 26 GHz–1.1 THz using time-domain spectroscopy," *J. Infr., Millim., THz Waves*, vol. 40, no. 2, pp. 210–218, Feb. 2019.

[27] B. Ghassemiparvin and N. Ghalichechian, "Reconfigurable antennas: Quantifying payoffs for pattern, frequency, and polarisation reconfiguration," *IET Microw., Antennas Propag.*, vol. 14, no. 3, pp. 149–153, Feb. 2020.

[28] N. Behdad and K. Sarabandi, "A varactor-tuned dual-band slot antenna," *IEEE Trans. Antennas Propag.*, vol. 54, no. 2, pp. 401–408, Feb. 2006.

[29] B. Ghassemiparvin, S. Shah, and N. Ghalichechian, "Novel paraffin-based 100-GHz variable capacitors for reconfigurable antennas," in *Proc. 11th Eur. Conf. Antennas Propag. (EUCAP)*, Mar. 2017, pp. 3506–3510.

[30] B. Ghassemiparvin and N. Ghalichechian, "Paraffin-based RF microsystems for millimeter wave reconfigurable antennas," in *Proc. IEEE Int. Symp. Antennas Propag. USNC/URSI Nat. Radio Sci. Meeting*, Jul. 2019. [Online]. Available: https://www.usnc-ursi-archive.org/aps-ursi/2019/abstracts/1172.pdf

[31] R. Simons, *Coplanar Waveguide Discontinuities Circuit Elements*. Hoboken, NJ, USA: Wiley, 2002.

[32] Thermodynamics Research Center, NIST Boulder Laboratories, and Kenneth Kroenlein Director, "Thermodynamics source database," in *NIST Chemistry WebBook, NIST Standard Reference Database Number 69*, P. J. Linstrom and W. G. Mallard, Eds. Gaithersburg, MD, USA: National Institute of Standards and Technology, 2018.

[33] S. Shah, B. Ghassemiparvin, and N. Ghalichechian, "Robust spin coating deposition process for paraffin phase-change films," *Microelectronic Eng.*, vol. 217, Sep. 2019, Art. no. 111121.

[34] J. P. Dunsmore, *Handbook of Microwave Component Measurements*. Hoboken, NJ, USA: Wiley, 2012.

[35] C. Matos, J. Li, and N. Ghalichechian, "Robotically controlled pattern measurements of 60 GHz phased array antenna," in *Proc. Antenna Meas. Techn. Assoc. Symp. (AMTA)*, Oct. 2019, pp. 1–2.

Behnam Ghassemiparvin (Member, IEEE) received the B.S. degree in electrical engineering-telecommunication from the University of Tabriz, Tabriz, Iran, in 2010, the M.S. degree in electrical and electronics engineering from Bilkent University, Ankara, Turkey, in 2012, and the Ph.D. degree in electrical and computer engineering from The Ohio State University, Columbus, OH, USA, in 2020. He was a Graduate Research Associate with the ElectroScience Laboratory, The Ohio State University, from 2014 to 2019. In 2020, he joined Apple Inc., Cupertino, CA, USA, as an Antenna Design Engineer. His research interests include design, microfabrication and testing of millimeter-wave reconfigurable antennas, paraffin-based thermo-electro-mechanical systems, and complex permittivity characterization of materials using time-domain spectroscopy. He was a recipient of the URSI Young Scientist Award in 2014.

Nima Ghalichechian (Senior Member, IEEE) received the Ph.D. degree in electrical engineering from the University of Maryland, College Park, in 2007. He developed MEMS electrostatic micromotors supported on microball bearings at the University of Maryland. From 2007 to 2012, he was a Senior Principal Engineer with the Research Department, FormFactor Inc., Livermore, CA, USA. During this period, he helped to design and develop MEMS microsprings for advanced probe cards used in testing memory and SoC semiconductor devices. In 2012, he joined The Ohio State University as a Research Scientist. As a Principal Investigator, he established several new programs sponsored by NSF, DARPA, and AFRL. From 2016 to 2017, he held a research assistant professor position. He transitioned into an assistant professor position in August 2017. He is currently an Assistant Professor with the Department of Electrical and Computer Engineering and the ElectroScience Laboratory at The Ohio State University. He is a Principal Investigator and the Director of the RF Microsystems Laboratory and advises seven Ph.D. and two master's students. His research interests include phase-change materials, reconfigurable antennas, arrays, UWB antennas, millimeter-wave systems, meta-surfaces, 3-D-printed antennas, novel materials, and microfabrication techniques. He was a recipient of the 2019 NSF CAREER Award, the 2019 Air Force Research Laboratory Summer Faculty Fellowship Award, and the 2018 Ohio State University Lumley Research Award.